Two-photon transport through a waveguide coupling to a whispering-gallery resonator containing an atom and photon-blockade effect

T. Shi (石弢)[1] and Shanhui Fan (范汕洄)[2]

[1]*Max-Planck-Institut für Quantenoptik, Hans-Kopfermann-Strasse. 1, 85748 Garching, Germany*

[2]*Ginzton Laboratory, Department of Electrical Engineering, Stanford University, Stanford, California 94305, USA*

(Received 21 August 2012; published 13 June 2013)

We investigate the two-photon transport through a waveguide side coupling to a whispering-gallery-atom system. Using the Lehmann-Symanzik-Zimmermann reduction approach, we present the general formula for the two-photon processes including the two-photon scattering matrices, the wave functions, and the second order correlation functions of the outgoing photons. Based on the exact results of the second order correlation functions, we analyze the quantum statistics behaviors of the outgoing photons for two different cases: (a) the ideal case without the intermodal coupling in the whispering-gallery resonator; and (b) the case in the presence of the intermodal coupling which leads to more complex nonlinear behavior. In the ideal case, we show that the system consists of two independent scattering pathways, a free pathway by a cavity mode without atomic excitation, and a "Jaynes-Cummings" pathway described by the Jaynes-Cummings Hamiltonian of a single-mode cavity coupling to an atom. The presence of the free pathway leads to two-photon correlation properties that are distinctively different from the standard Jaynes-Cummings model, in both the strong and weak-coupling regime. In the presence of intermodal mixing, the system no longer exhibits a free resonant pathway. Instead, both the single-photon and the two-photon transport properties depend on the position of the atom. Thus, in the presence of intermodal mixing, one can in fact tune the photon correlation properties by changing the position of the atom. Our formalism can be used to treat resonator and cavity dissipation as well.

DOI: 10.1103/PhysRevA.87.063818 PACS number(s): 42.50.Ct, 42.79.Gn, 11.55.Ds

I. INTRODUCTION

Recently, the whispering-gallery-atom system has inspired a lot of interest [1–11], owing to its broad applications in the studies of quantum optics. A schematic of such a systemis shown in Fig. 1, where a waveguide is side coupled to a whispering-gallery resonator, which then couples to a two-level system. In the experimental study of this system [2–4], the two-level system can be either a quantum dot [2], or an actual atom [3]. Here, we will refer to such a two-level system as an "atom."These experiments have measured the transmission properties of such a waveguide-resonator-atom system under weak light excitation, and have demonstrated quantum effects including antibunching and photon-blockade effects.

The experimental progress on this system, in turn, motivated several recent theoretical studies. Srinivasan and Painter analyzed this system under the excitation of a weak coherent state input [12], and obtained transmission and coherence properties through a numerical procedure with a truncated number-state basis for the photons in the resonator [5]. Shen and Fan calculated analytically the transmission properties of such a resonator system with an input of a single-photon Fock state [6,7]. Subsequently, the single-photon transports in the whispering-gallery system have been extensively studied [8–11].

In this paper, we study the two-photon transport property of this system shown in Fig. 1. While the response of the system under weak coherent-state input yields much information about its nonclassical properties, we note that one important goal of integrated quantum optics is to process quantum states. Therefore, it is important to study such a system with the input of nonclassical states, such as the Fock state, as well. In addition, in contrast to the study of the transport properties of a single photon [13–18], the studies of two-photon transports provide important information [19–28] about atom-induced photon-photon interaction that is absent in the single-photon Hilbert space.

Our work provides contributions to the literature of cavity quantum electrodynamics (QED) [29,30]. Unlike the standard Jaynes-Cummings (JC) system where a two-level atom couples to a single-cavity mode [31], the whispering-gallery resonator supports two modes, both of which may couple to the atom. The simultaneous presence of both modes results in transport and correlation properties that can be significantly different as compared to the standard single-mode JC system [6,7]. One of our contributions here is to illustrate, in the two-photon Hilbert space, the connection and the difference of the present system from the standard Jaynes-Cumming system.

The paper is organized as follows. In Secs. II and III, we review the model Hamiltonian and our theoretical approach based on the Lehmann-Symanzik-Zimmermann (LSZ) reduction formula in quantum field theory [32]. This approach results in an exact formula for the scattering matrix of the system in multiphoton subspace. In Sec. IV, we present the exact analytical results, including the single-photon transmissions and the wave functions for the two outgoing photons. Based on the general analytical results, we analyze the very distinct quantum statistics behaviors of the outgoing photons for two different cases of the strong coupling case in Secs. V and VI. Section V considers the ideal case in the absence of intermodal coupling in the whispering-gallery resonator. Section VI analyzes the effect of intermodal coupling which leads to more complex nonlinear behavior. In Sec. VII, the results are summarized with some remarks and outlooks.

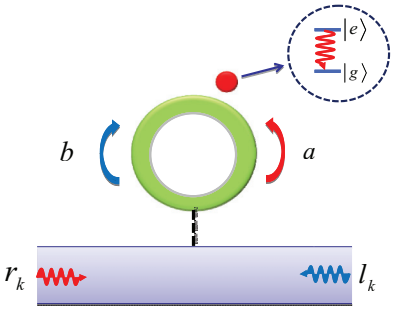

FIG. 1. (Color online) The schematics for the system: The blue (left) and red (right) arrows denote the two whispering-gallery modes, which interact with the atom and the waveguide.

II. MODEL SETUP

The system in Fig. 1 is described by the Hamiltonian [6,7]

$$H = H_{\rm W} + H_{\rm wg} + H_{\rm hyb}. \tag{1}$$

Here,

$$H_{\rm W} = \sum_{k>0} k r_k^\dagger r_k - \sum_{k<0} k l_k^\dagger l_k \tag{2}$$

describes photons propagating in the waveguide. r_k ($r_k^\dagger$) and l_k ($l_k^\dagger$) are the annihilation (creation) operators of right-moving and left-moving photons, respectively. The right-moving photons have momentum $k > 0$, and the left-moving photons have momentum $k < 0$. Here, one linearizes the waveguide dispersion relation around the operating frequency. The group velocity can then be taken to be unity by a rescaling of the corresponding operator. A detailed derivation that justifies this Hamiltonian with the linearized dispersion can be found in Ref. [6].

In Eq. (1)

$$H_{\rm wg} = \Omega|e\rangle\langle e| + \omega_c(a^\dagger a + b^\dagger b) + h b^\dagger a + h^* a^\dagger b + \sigma^+(g_a a + g_b b) + \text{H.c.} \tag{3}$$

describes the two-level system, the resonator, and the interaction between them under the rotating-wave approximation. In Eq. (3), a and b are the annihilation operators for the two counterrotating modes in the resonator. h is the strength of intermodal coupling between these two modes and is typically induced by surface roughness on the resonator. The atom supports a ground state $|g\rangle$ and an excited state $|e\rangle$ with a transition frequency Ω. g_a (g_b) is the coupling constant between mode a (b) and the atom, and $\sigma^+ = |e\rangle\langle g|$.

In Eq. (1),

$$H_{\rm hyb} = \frac{1}{\sqrt{L}} \sum_k (V_R r_k^\dagger a + V_L l_k^\dagger b + \text{H.c.}) \tag{4}$$

describes the coupling between the waveguide and the resonator. Here, we adopt a box-normalization scheme with L being the length of the waveguide, and V_R (V_L) is the coupling strength between the right-moving (left-moving) photon in the waveguide and the mode a (b) in the whispering-gallery system. The waveguide-cavity coupling results in a cavity loss rate $\Gamma_{\rm tot} = \Gamma_R + \Gamma_L$, where $\Gamma_{R,L} = |V_{R,L}|^2$ being the decay rates of the two whispering-gallery modes to the waveguide, respectively. We ignore all other possible loss mechanisms.

We end this section by briefly commenting on various experimental aspects that are related to the Hamiltonian of Eq. (1). As a representative example, the experiment in Refs. [2–4] has $\omega_c \sim \Omega \sim 10^6$ GHz. The resonator linewidth $\Gamma_{tot}/2\pi = 0.1$ to 10 MHz. The atom-resonator coupling constant $|g_i|/2\pi$ ($i = a,b$) can reach 1 MHz to 10 GHz. We quote these numbers to provide a rough sense of the parameters involved here. The theory does not depend on such a detailed choice of parameters. We will consider both the strong coupling regime, where $|g_i| \gg \Gamma_{tot}$, and the weak coupling regime, where $|g_i| \ll \Gamma_{tot}$.

In the experiment in Ref. [3] the intermodal mixing has a strength of $|h|/2\pi = 1$ to 100 MHz. The phase of the h depends on the detail of the surface roughness and typically cannot be controlled in an experiment. On the other hand, the relative phase of g_a and g_b depends on the position of the atom, which can be controlled experimentally [6,7]. Since the size of the whispering-gallery mode is at least a few wavelengths, the relative phase of g_a and g_b can vary anywhere between 0 and 2π.

III. OVERVIEW OF THE THEORETICAL APPROACH

We solve the single- and two-photon scattering matrix (S matrix) for the Hamiltonian in Eq. (1) using the LSZ approach. This approach has been discussed in detail in Refs. [23,24]. Here we only provide a brief summary of those aspects that are relevant for subsequent discussions.

The single-photon and two-photon S matrices read

$$S_{p;k} = \delta_{kp} + i T_{p;k} \tag{5}$$

and

$$S_{p_1p_2;k_1k_2} = S_{p_1k_1} S_{p_2k_2} + S_{p_2k_1} S_{p_1k_2} + i T_{p_1p_2;k_1k_2}, \tag{6}$$

respectively, where k (p) is the momentum of the incident (outgoing) single photon, and k_1, k_2 (p_1, p_2) are the momenta of two incident (outgoing) photons. The right- and left-moving photons have the positive and negative momenta, respectively. Here, the T-matrix element $T_{p_1,\ldots,p_n;k_1,\ldots,k_n} \equiv T_{[\mathbf{p};\mathbf{k}]}$ has the form

$$i T_{[\mathbf{p};\mathbf{k}]} = \lim_{\substack{\omega_{k_j}\to k_j,\\ \omega_{p_j}\to p_j}} \frac{(2\pi)^n G_{[\mathbf{p};\mathbf{k}]}(\omega_{\mathbf{p}},\omega_{\mathbf{k}})}{\prod_{j=1}^n [G_0(\omega_{k_j},k_j) G_0(\omega_{p_j},p_j)]}. \tag{7}$$

In Eq. (7), $G_0(\omega,k) = i/(\omega - \varepsilon_k + i0^+)$ is the free propagator of a single photon with $\varepsilon_k = |k|$ being the dispersion relation of the waveguide.

$$G_{[\mathbf{p};\mathbf{k}]}(\omega_{\mathbf{p}},\omega_{\mathbf{k}}) = \int \prod_{j=1}^n \left[\frac{dt_j dt_j'}{2\pi}\right] G_{[\mathbf{p};\mathbf{k}]}(\mathbf{t}',\mathbf{t}) \times \prod_{j=1}^n [\exp(i\omega_{p_j} t_j' - i\omega_{k_j} t_j)] \tag{8}$$

is the Fourier transform of the exact Green function $G_{[\mathbf{p};\mathbf{k}]}(\mathbf{t}',\mathbf{t})$. Such a Green function can be determined

as

$$G_{[\mathbf{p};\mathbf{k}]}(\mathbf{t}',\mathbf{t}) = \frac{(-)^n \delta^{2n} \ln Z[\eta_k,\eta_k^*]}{\delta\eta^*_{f,p_1}(t_1')\cdots\delta\eta^*_{f,p_n}(t_n')\delta\eta_{f,k_1}(t_1)\cdots\delta\eta_{f,k_n}(t_n)}\Bigg|_{\substack{\eta_{f,k}=0\\ \eta^*_{f,k}=0}}, \tag{9}$$

where

$$Z[\eta_k,\eta_k^*] = \int D[\text{field}]\exp(iS_c + iS_{ex}) \tag{10}$$

is the generating functional in the path integral formalism. Here, $\int D[\text{field}]$ denotes the path integral over all fields in the system, S_c is the action of the system, and

$$S_{ex} = \sum_{f=r,l}\int dt \sum_k [\eta^*_{f,k}(t) f_k(t) + \text{H.c.}] \tag{11}$$

describes the external sources $\eta_{f,k}(t)$ that injects photons into the waveguide.

Based on the formalism as outlined above, in the next section we show the exact analytical results for the single-photon and two-photon scattering processes.

IV. ANALYTIC RESULTS FOR ONE- AND TWO-PHOTON *S* MATRICES

In this section, the S matrices are obtained by LSZ reduction, which leads to the exact results of the single-photon transmission and the second order correlation functions of the two outgoing photons.

A. Single-photon transport

For the single-photon case, using the T-matrix element (7), the Green function (9), and the generating functional (10), we obtain

$$S_{p;k} = T_k\delta_{p,k} + R_k\delta_{p,-k}, \tag{12}$$

where

$$T_k = 1 - i|V_R|^2\langle 0|a\frac{1}{k - H_{\text{eff}}}a^\dagger|0\rangle \tag{13}$$

and

$$R_k = -iV_LV_R^*\langle 0|b\frac{1}{k - H_{\text{eff}}}a^\dagger|0\rangle \tag{14}$$

are the transmission and reflection coefficients, respectively. Here,

$$H_{\text{eff}} = \Omega|e\rangle\langle e| + \left(\omega_c - i\frac{\Gamma_R}{2}\right)a^\dagger a + \left(\omega_c - i\frac{\Gamma_L}{2}\right)b^\dagger b + hb^\dagger a + \sigma^+(g_a a + g_b b) + \text{H.c.}, \tag{15}$$

is the effective Hamiltonian. Without loss of generality, we consider $\Gamma_R = \Gamma_L \equiv \Gamma$. We notice that the excitation number $N = |e\rangle\langle e| + a^\dagger a + b^\dagger b$ commutes with H_{eff}. Thus, for single-photon scattering, in the single-excitation subspace as spanned by the basis $\{|e\rangle|0\rangle_a|0\rangle_b, |g\rangle|1\rangle_a|0\rangle_b, |g\rangle|0\rangle_a|1\rangle_b\}$, we represent the effective Hamiltonian as

$$H^{(1)}_{\text{eff}} = \begin{pmatrix} \Omega & g_a & g_b \\ g_a^* & \omega_c - i\frac{\Gamma}{2} & h^* \\ g_b^* & h & \omega_c - i\frac{\Gamma}{2} \end{pmatrix}. \tag{16}$$

Using Eq. (16), the single-photon reflection and transmission coefficients can be determined as

$$R_k = \frac{-iV_LV_R^*}{D(k)}[g_ag_b^* + h(k-\Omega)] \tag{17}$$

and

$$T_k = 1 - \frac{i\Gamma}{D(k)}\left[(k-\Omega)\left(k - \omega_c + i\frac{\Gamma}{2}\right) - |g_b|^2\right], \tag{18}$$

respectively. Here, we define

$$D(k) = \left(k - \omega_c + i\frac{\Gamma}{2}\right)\left[(k-\Omega)\left(k-\omega_c+i\frac{\Gamma}{2}\right) - G_+^2\right] - g_a^*g_bh - g_b^*g_ah^* - |h|^2(k-\Omega), \tag{19}$$

and

$$G_+ = \sqrt{|g_a|^2 + |g_b|^2}. \tag{20}$$

The results (17) and (18) accord with that obtained in Refs. [6,7].

Equations (17) and (18) are applicable in the absence of intrinsic atomic or cavity dissipation. In the presence of intrinsic dissipations, the reflection and transmission probabilities $|R_k|^2$ and $|T_k|^2$ are obtained by substitutions $\Omega - i\gamma_a$ and $\omega_c - i\gamma_c$ for Ω and ω_c in Eqs. (17) and ((18)), where γ_a and γ_c are the intrinsic decay rates of the atom and the cavity, respectively.

B. Two-photon transport

In the subsection, we derive the exact formula for the scattering wave functions and the second-order correlation functions of two outgoing photons by the LSZ reduction approach. By evaluating Eqs. (7), (9), and (10), we obtain the S-matrix elements in the two-photon Hilbert space:

$$S^{(\text{R})}_{p_1p_2;k_1k_2} = R_{k_1}R_{k_2}(\delta_{p_1,-k_1}\delta_{p_2,-k_2} + \delta_{p_1,-k_2}\delta_{p_2,-k_1}) - i\frac{V_L^2V_R^{*2}}{2\pi}\delta_{p_1+p_2,-k_1-k_2}U_{p_1p_2;k_1k_2} \tag{21}$$

and

$$S^{(\text{T})}_{p_1p_2;k_1k_2} = T_{k_1}T_{k_2}(\delta_{p_1,k_1}\delta_{p_2,k_2} + \delta_{p_1,k_2}\delta_{p_2,k_1}) - i\frac{|V_R|^4}{2\pi}\delta_{p_1+p_2,k_1+k_2}W_{p_1p_2;k_1k_2} \tag{22}$$

for two reflected photons and two transmitted photons. In Eqs. (21) and (22),

$$U_{p_1p_2;k_1k_2} = F_1(p_1,p_2;k_1,k_2) + F_1(p_1,p_2;k_2,k_1) + F_1(p_2,p_1;k_1,k_2) + F_1(p_2,p_1;k_2,k_1) \tag{23}$$

and

$$W_{p_1p_2;k_1k_2} = F_2(p_1,p_2;k_1,k_2) + F_2(p_1,p_2;k_2,k_1) + F_2(p_2,p_1;k_1,k_2) + F_2(p_2,p_1;k_2,k_1). \tag{24}$$

Here, we define

$$F_1(p_1,p_2;k_1,k_2) = \langle 0|b\frac{1}{-p_1-H_{\rm eff}^{(1)}}b\frac{1}{k_1+k_2-H_{\rm eff}^{(2)}}a^\dagger\frac{1}{k_2-H_{\rm eff}^{(1)}}a^\dagger|0\rangle + \frac{1}{-p_1-k_1}\langle 0|b\frac{1}{-p_1-H_{\rm eff}^{(1)}}a^\dagger b\frac{1}{k_2-H_{\rm eff}^{(1)}}a^\dagger|0\rangle \quad (25)$$

and

$$F_2(p_1,p_2;k_1,k_2) = \langle 0|a\frac{1}{p_1-H_{\rm eff}^{(1)}}a\frac{1}{k_1+k_2-H_{\rm eff}^{(2)}}a^\dagger\frac{1}{k_2-H_{\rm eff}^{(1)}}a^\dagger|0\rangle + \frac{1}{p_1-k_1}\langle 0|a\frac{1}{p_1-H_{\rm eff}^{(1)}}a^\dagger a\frac{1}{k_2-H_{\rm eff}^{(1)}}a^\dagger|0\rangle, \quad (26)$$

where $H_{\rm eff}^{(1)}$ is defined in Eq. (16). In the two-excitation subspace as spanned by the basis $\{|g\rangle|2\rangle_a|0\rangle_b, |e\rangle|1\rangle_a|0\rangle_b, |g\rangle|1\rangle_a|1\rangle_b, |e\rangle|0\rangle_a|1\rangle_b, |g\rangle|0\rangle_a|2\rangle_b\}$, we represent the effective Hamiltonian

$$H_{\rm eff}^{(2)} = \begin{pmatrix} 2\alpha & \sqrt{2}g_a^* & \sqrt{2}h^* & 0 & 0 \\ \sqrt{2}g_a & \alpha+\Omega & g_b & h^* & 0 \\ \sqrt{2}h & g_b^* & 2\alpha & g_a^* & \sqrt{2}h^* \\ 0 & h & g_a & \alpha+\Omega & \sqrt{2}g_b \\ 0 & 0 & \sqrt{2}h & \sqrt{2}g_b^* & 2\alpha \end{pmatrix}, \quad (27)$$

where $\alpha = \omega_c - i\Gamma/2$. In general, direct evaluation of $U_{p_1p_2;k_1k_2}$ and $W_{p_1p_2;k_1k_2}$ can be rather complicated. However, there are cases where $U_{p_1p_2;k_1k_2}$ and $W_{p_1p_2;k_1k_2}$ can be obtained exactly in a compact form. We will discuss such examples in the next section.

The Fourier transformations of matrix elements (21) and (22) result in wave functions of the two reflected or transmitted photons:

$$\psi_{\rm R}(x_1,x_2) = \frac{1}{4\pi}\int dp_1dp_2S^{\rm (R)}_{p_1p_2;k_1k_2}e^{ip_1x_1+ip_2x_2} = \frac{1}{2\pi}e^{-iEx_c}\left[R_{k_1}R_{k_2}\cos(\Delta_k x) + \frac{1}{2}V_L^2V_R^{*2}\int\frac{d\Delta_p}{2\pi i}e^{i\Delta_p x}U_{p_1p_2;k_1k_2}\right] \quad (28)$$

and

$$\psi_{\rm T}(x_1,x_2) = \frac{1}{4\pi}\int dp_1dp_2S^{\rm (T)}_{p_1p_2;k_1k_2}e^{ip_1x_1+ip_2x_2} = \frac{1}{2\pi}e^{iEx_c}\left[T_{k_1}T_{k_2}\cos(\Delta_k x) + \frac{1}{2}|V_R|^4\int\frac{d\Delta_p}{2\pi i}e^{i\Delta_p x}W_{p_1p_2;k_1k_2}\right], \quad (29)$$

respectively. Here, we define the total momentum $E = k_1 + k_2 = p_1 + p_2$, the relative momenta $\Delta_k = (k_1 - k_2)/2$ and $\Delta_p = (p_1 - p_2)/2$, as well as the center of mass coordinate $x_c = (x_1 + x_2)/2$ and the relative coordinate $x = x_1 - x_2$. Because $U_{p_1p_2;k_1k_2}$ and $W_{p_1p_2;k_1k_2}$ are both even functions of Δ_p, $\psi_{\rm R}(x_1,x_2)$ and $\psi_{\rm T}(x_1,x_2)$ are invariant under the permutation $x_1 \longleftrightarrow x_2$, as required since photons are bosons. From now on, we only focus on the wave functions for $x > 0$.

The integral in Eqs. (28) and (29) can be evaluated by analyzing the analytic properties of the matrix elements $U_{p_1p_2;k_1k_2}$ and $W_{p_1p_2;k_1k_2}$. These matrix elements exhibit three poles $p_l = E/2 - \alpha_l$ on the upper half plane, where α_l is the eigenvalue of $H_{\rm eff}^{(1)}$ with $l = 1,2,3$. Here, notice that the eigenvalues of $H_{\rm eff}^{(2)}$ do not contribute to the poles in $U_{p_1p_2;k_1k_2}$ and $W_{p_1p_2;k_1k_2}$, because they only associate with the total energy E, as shown in Eqs. (25) and (26), and we consider here an incident two-photon state with a fixed total energy. The residue theorem then leads to the wave functions

$$\psi_{\rm R}(x_1,x_2) = \frac{1}{2\pi}e^{-iEx_c}\left[R_{k_1}R_{k_2}\cos(\Delta_k x) + \frac{1}{2}V_L^2V_R^{*2}\sum_l {\rm Res}_{p_l}U_{p_1p_2;k_1k_2}e^{ip_lx}\right] \quad (30)$$

and

$$\psi_{\rm T}(x_1,x_2) = \frac{1}{2\pi}e^{iEx_c}\left[T_{k_1}T_{k_2}\cos(\Delta_k x) + \frac{1}{2}|V_R|^4\sum_l {\rm Res}_{p_l}W_{p_1p_2;k_1k_2}e^{ip_lx}\right], \quad (31)$$

where ${\rm Res}_{p_l}W(U)_{p_1p_2;k_1k_2}$ denotes the residue of the function $W(U)_{p_1p_2;k_1k_2}$ at $(p_1 - p_2)/2 = p_l$.

From the two-photon wave functions, the second-order correlations functions for the reflected and transmitted photons can be obtained as

$$g_{\rm R}^{(2)}(\tau) = \frac{\langle\psi_{\rm R}|l^\dagger(x)l^\dagger(x+\tau)l(x+\tau)l(x)|\psi_{\rm R}\rangle}{|\langle\psi_{\rm R}|l^\dagger(x)l(x)|\psi_{\rm R}\rangle|^2}, \quad g_{\rm T}^{(2)}(\tau) = \frac{\langle\psi_{\rm T}|r^\dagger(x)r^\dagger(x+\tau)r(x+\tau)r(x)|\psi_{\rm T}\rangle}{|\langle\psi_{\rm T}|r^\dagger(x)r(x)|\psi_{\rm T}\rangle|^2}, \quad (32)$$

where $r(x)$ $[l(x)]$ is the Fourier transformation of r_k (l_k). Equation (32) can be simplified to yield $g_s^{(2)}(\tau) = |\psi_s(x+\tau,x)|^2/\int dy|\psi_s(x,y)|^2$, where s denote "R and "T. Therefore, our theoretical results on the two-photon wave functions can be compared to the experimental measurement of second-order correlation functions for this system.

In the presence of intrinsic atomic or cavity dissipation, Eqs. (30) and (31) remain valid, provided that we substitute $\Omega - i\gamma_{\rm a}$ and $\omega_c - i\gamma_{\rm c}$ for Ω and ω_c in $U_{p_1p_2;k_1k_2}$ and $W_{p_1p_2;k_1k_2}$.

C. Spectrum of the whispering-gallery-atom system

For this system, its transport properties are closely related to the spectrum of the resonator coupling to the atom. Therefore, in this section we provide a brief discussion of the spectrum of the resonator-atom Hamiltonian $H_{\rm wg}$ as defined in Eq. (3). We consider two separate cases:

Case (a). As seen in Eq. (3), the whispering-gallery resonator by itself supports a clockwise and a counterclockwise rotating mode, both coupled to the atom. However, assuming that either

$$h = 0, \quad (33)$$

or

$$h \neq 0, \text{ and } \frac{g_b}{g_a} = \pm e^{-i\theta_h}, \quad (34)$$

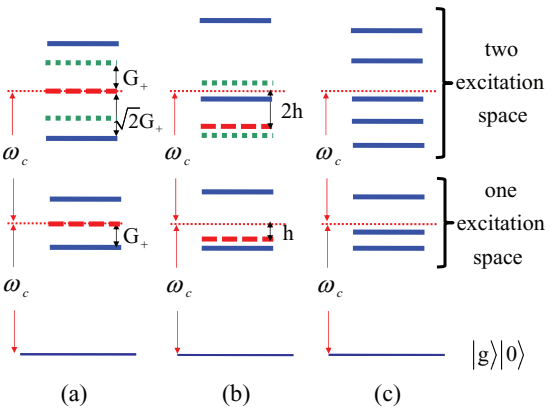

FIG. 2. (Color online) The schematics for the energy spectra of the whispering-gallery-atom system, where Γ is taken as unity. (a) $h = 0$; (b) $h = 2e^{i\theta_h}$, and $g_b/g_a = e^{-i\theta_h}$; (c) $h = 5i$ and $g_b/g_a = 1$. (a) and (b) correspond to the effective single mode case, and (c) corresponds to the two mode case. In all panels, thin blue lines at the bottom represent the ground state. Red dashed lines represent a free mode without atomic excitation. Notice that it forms a linear spectrum. Green dotted lines represent a mode that consists of one excitation in the free mode, and one excitation in the JC mode. Solid blue lines represent all other modes.

it is then possible to form a linear superposition of these modes that is decoupled from the atom. In Eq. (34), $\theta_h = \arg h$ is the phase of h. In either case, the resonator-atom Hamiltonian can be rewritten as:

$$H_{\text{eff}} = \Omega|e\rangle\langle e| + \omega_A A^\dagger A + \omega_B B^\dagger B + (G_+\sigma^+ A + \text{H.c.}), \tag{35}$$

where the operators $A = (g_a a + g_b b)/G_+$ and $B = (g_b^* a - g_a^* b)/G_+$. For the case described by Eq. (33), we have $\omega_A = \omega_B = \omega_c - i\Gamma/2$. For the case described by Eq. (34), we have $\omega_A = \omega_c - i\Gamma/2 \pm |h|$ and $\omega_B = \omega_c - i\Gamma/2 \mp |h|$.

It follows from Eq. (35) that the mode B is decoupled form the atom, while mode A couples to the atom through the standard JC Hamiltonian

$$H_{\text{JC}} = \Omega|e\rangle\langle e| + \omega_A A^\dagger A + (G_+\sigma^+ A + \text{H.c.}). \tag{36}$$

For subsequent discussion, we refer to mode A as the "JC mode" and mode B as the "free mode,"respectively.

The spectrum of the Hamiltonian (35) is displayed in Fig. 2(a) for the case $h = 0$, and in Fig. 2(b) for the case when $h \neq 0$, and $g_b/g_a = \pm e^{-i\theta_h}$. In either case, due to the very different nature of modes A and B, for the incident photons with energy on resonance with modes A and B, the outgoing photons must exhibit very different statistics behaviors, which could be investigated by the second order correlation functions $g_s^{(2)}(\tau)$.

Case (b). When neither conditions in Eq. (33) nor Eq. (34) are satisfied, we can no longer form a linear superposition of the two whispering-gallery modes that decouples with the atom. The energy spectrum, shown in Fig. 2(c), is more complicated.

In the next two sections, we study the photon transmissions for the cases (a) and (b), respectively. In case (a), the atom effectively couples only to one of the two modes of the resonator, below we refer to this case as an "effective single-mode case."In contrast, for case (b) the atom couples to both modes, and below we refer to this case as a "two-mode case."

V. RESULTS FOR THE EFFECTIVE SINGLE-MODE CASE

In this section, we present transport properties of a single photon and two photons, for the effective single-mode case as discussed in Section III C, where the resonator supports a photon mode that is decoupled from the atom. For the numerical results in this and the next section, we normalize all quantities that have the dimension of energy with respect to Γ, the waveguide-resonator coupling rate. Also, we choose ω_c as the origin of the energy axis.

A. Single-photon transport

For this effective single-mode case, the single-photon reflection coefficient (14) can be rewritten as

$$R_k = -i\frac{\Gamma g_a g_b^*}{G_+^2}\left[\frac{k-\Omega}{(k-\Omega)(k-\omega_A) - G_+^2} - \frac{1}{k-\omega_B}\right], \tag{37}$$

in which the first and second terms describe the contributions from the JC mode and the free mode, respectively. We show the single-photon reflection and transmission probabilities $|R_k|^2$ and $|T_k|^2$ in Fig. 3.

Figures 3(a) and 3(b) correspond to the strong coupling case where $\Gamma \ll G_+$. In Fig. 3(a), we choose $h = 0$, $\Omega = \omega_c$, and $|g_a| = |g_b|$. There are three peaks in the reflection spectrum. The peak in the center of the spectrum corresponds to the free mode B. Two other peaks correspond to the JC modes in the single-excitation subspace.

In Fig. 3(b), we choose $\Omega = \omega_c + |h|$ and $g_b/g_a = e^{-i\theta_h}$. The reflection spectrum again exhibits three peaks. The central peak again corresponds to the free mode. Compared to the free mode in Fig. 3(a) at the frequency ω_c, here the frequency of the free mode is shifted to $\omega_c - |h|$ due to the intermodal coupling. The other two peaks correspond to the two JC modes.

In Fig. 3(c), we consider the weak coupling case. The transmission spectrum exhibits a single dip, and the reflection spectrum exhibits a single peak, at the atomic frequency.

Based on these results, we conclude that the single-photon transport consists of two independent scattering processes, i.e., the scattering by the JC modes, which have atomic excitation, and by the free mode that is decoupled from the atom.

B. Two-photon transport

For this effective single-mode case, straightforward calculations of Eqs. (25) and (26) lead to the analytic results

$$U_{p_1p_2;k_1k_2} = -\frac{2g_b^{*2}g_a^2(E-\omega_A-\Omega)}{\prod_{s=\pm}(E-\lambda_{2s})} \times \frac{(E-2\Omega)(E-2\omega_A) - 4G_+^2}{\prod_{s=\pm}\prod_{i=1,2}(k_i-\lambda_{1s})(p_i+\lambda_{1s})} \tag{38}$$

and

$$W_{p_1p_2;k_1k_2} = -\frac{2|g_a|^4(E-\omega_A-\Omega)}{\prod_{s=\pm}(E-\lambda_{2s})} \times \frac{(E-2\Omega)(E-2\omega_A) - 4G_+^2}{\prod_{s=\pm}\prod_{i=1,2}(k_i-\lambda_{1s})(p_i-\lambda_{1s})}. \tag{39}$$

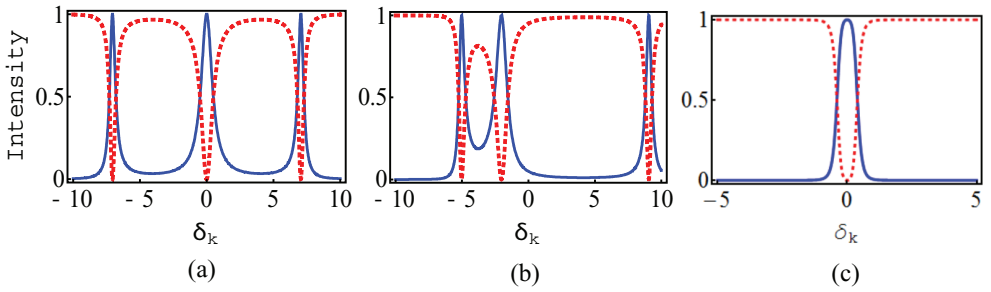

FIG. 3. (Color online) Single-photon transmission (red dashed curve) and reflection (blue solid curve) spectra for the effective single-mode case. All quantities with energy dimensions are normalized to Γ, and δ_k is the detuning between the incident photon and ω_c : (a) $h = 0$, $|g_a| = |g_b| = 5$, and $\Omega = \omega_c$; (b) $|h| = 2$, $|g_a| = |g_b| = 5$, $g_b/g_a = e^{-i\theta_h}$, and the detuning $\Omega - \omega_c = 2$ between the atom and the cavity; and (c) $h = 0$, $|g_a| = |g_b| = 0.3$, and $\Omega = \omega_c$.

Here, $\lambda_{1\pm}$ and $\lambda_{2\pm}$ are the eigenvalues of $H_{\rm JC}$ in the single- and two-excitation subspaces [24]. Together with Eqs. (38) and (39), it follows from Eqs. (30) and (31) that the wave functions of the reflected and transmitted photons are

$$\psi_{\rm R}(x_1,x_2) = \frac{e^{-iEx_c}}{2\pi}\left[R_{k_1}R_{k_2}\cos(\Delta_k x) - V_L^2 V_R^{*2} g_b^{*2} g_a^2 F(x)\right] \tag{40}$$

and

$$\psi_{\rm T}(x_1,x_2) = \frac{e^{iEx_c}}{2\pi}[T_{k_1}T_{k_2}\cos(\Delta_k x) - |V_R|^4|g_a|^4 F(x)], \tag{41}$$

respectively, where we define

$$F(x) = \frac{\sum_s s(E-2\lambda_{1s})e^{i(\frac{E}{2}-\lambda_{1-s})|x|}}{\prod_{s=\pm}[(E-\lambda_{2s})\prod_{i=1,2}(k_i-\lambda_{1s})](\lambda_{1+}-\lambda_{1-})}. \tag{42}$$

The second-order correlation

$$g_{\rm R}^{(2)}(\tau) = \left|1 - \frac{V_L^2 V_R^{*2} g_b^{*2} g_a^2 F(\tau)}{R_{E/2}^2}\right|^2 \tag{43}$$

of the two reflected photons is obtained by applying Eq. (32) to the wave functions determined from Eq. (40).

We note that $U_{p_1p_2;k_1k_2}$ and $W_{p_1p_2;k_1k_2}$, i.e., the two-photon correlated scattering, have contributions only from the JC modes. The free mode does not contribute to the functions of $U_{p_1p_2;k_1k_2}$ and $W_{p_1p_2;k_1k_2}$. Nevertheless, the presence of such a free mode does strongly influence the transport properties. And as a result, the two-photon correlation properties are different in this system as compared to the case of the standard JC model analyzed in [24,27]. Below, using Eqs. (38), (39), and (43), we highlight such differences in both the strong and the weak coupling regimes.

C. Strong Coupling Case

Using the closed-form analytic results of the previous section, we now consider the two-photon transport properties, for the strong-coupling cases corresponding to the systems shown in Figs. 3(a) and 3(b).

The two-photon background fluorescence $B_R = |V_R|^4|V_L|^4|U_{p_1p_2;k_1k_2}|^2/4\pi^2$ of the reflected photons are shown in Fig. 4. B_R displays a single peak at $\Delta_k = \Delta_p = 0$ when the total energy of the incident photons approaches $2{\rm Re}\lambda_{1\pm}$ [Figs. 4(a) and 4(b)], while the two-photon background fluorescence splits into four peaks when the total energy of the incident photons deviates from $2{\rm Re}\lambda_{1\pm}$ [Figs. 4(c) and 4(d)].

In general, the background fluorescence peaks when one of the incident or outgoing photons has an energy that coincides with a single-excitation eigenstate [24]. Examining Eqs. (38) and (39), we see that the poles occur at $\Delta_k = \pm(E/2 - {\rm Re}\lambda_{1s})$ and $\Delta_p = \pm(E/2 - {\rm Re}\lambda_{1s})$. Thus, one might expect eight peaks in the background fluorescence spectra in the general

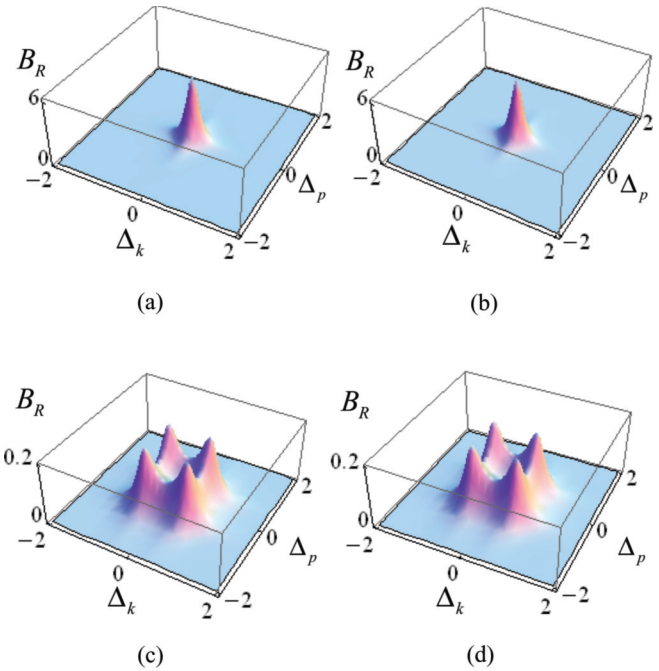

FIG. 4. (Color online) The two-photon background fluorescence for the effective single-mode case. All quantities with a dimension of energy are normalized with respect to Γ: (a) the system parameters are the same as those in Fig. 3(a), and the detuning $E - 2\omega_c = -14$; (b) the system parameters are the same as those in Fig. 3(b), and the detuning $E - 2\omega_c = -10$; (c) the system parameters are the same as those in Fig. 3(a), and the detuning $E - 2\omega_c = 13$; and (d) the system parameters are the same as those in Fig. 3(b), and the detuning $E - 2\omega_c = 17$.

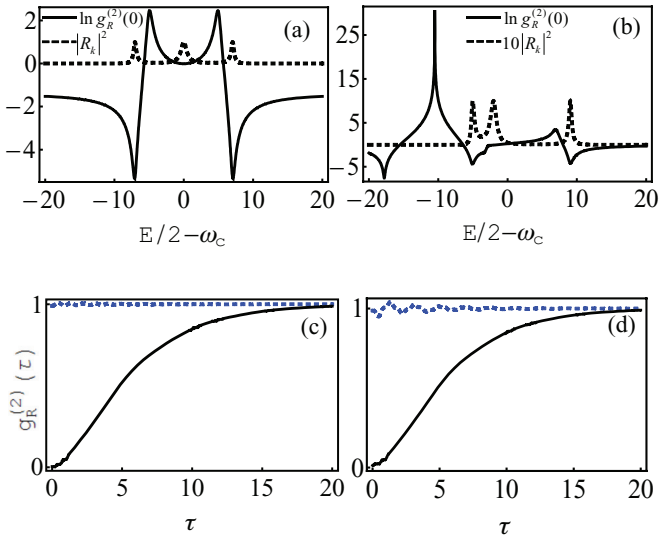

FIG. 5. (Color online) The second order correlation functions of two reflected photons for the effective single-mode case. The two incident photons have the same energy $E/2$. All quantities with a dimension of energy are normalized with respect to Γ, and the system parameters for the left and the right panels are the same as those in Figs. 3(a) and 3(b), respectively. In (a) and (b), the second order correlation function and the reflection coefficient are depicted by the solid and dashed curves, respectively. (c) The solid (black) and dashed (blue) curves denote $g_{\mathrm{R}}^{(2)}(\tau)$ for $E/2-\omega_c=\pm 7$ (a single photon being resonant with the JC mode) and $E/2-\omega_c=0$ (a single photon being resonant with the free mode), respectively. (d) The solid (black) and blue (dashed) curves denote $g_{\mathrm{R}}^{(2)}(\tau)$ for $E/2-\omega_c=-5{,}9$ (a single photon being resonant with the JC mode) and $E/2-\omega_c=-2$ (a single photon being resonant with the free mode), respectively.

case. However, four of these poles turn out to have very small residues, resulting in the presence of only four peaks in Figs. 4(c) and 4(d).

In Fig. 5, we plot the second-order correlation (43) for the two reflected photons. Here, we consider the same two systems in Fig. 3, and assume that the two incident photons have the same single-photon energy of $E/2$. Because $F(0)$ has the poles at $E/2=\lambda_{2\pm}/2$ and $\lambda_{1\pm}$, the Fig. 5(a) shows the two peaks at $\lambda_{2\pm}/2$ and two valleys at $\lambda_{1\pm}$. In Fig. 3, we saw that the systems exhibit strong resonant reflection for a single photon, when the single-photon energy is resonant with either the JC modes or the free modes. However, in the presence of two incident photons, the statistics of the outgoing photons at these resonances are very different. As we see in Fig. 5, when the single-photon energy coincides with the energy of one of JC modes, e.g., $E/2-\omega_c\sim -7$ in Fig. 5(c) and $E/2-\omega_c\sim -5$ in Fig. 5(d), we observe pronounced antibunching behavior with $g_{\mathrm{R}}^{(2)}(0)<g_{\mathrm{R}}^{(2)}(\tau)\leqslant 1$, and therefore a strong photon-blockade effect. On the other hand, neither the super-Possonian or the sub-Possonian light is generated when the single-photon energy coincides with that of the free mode, e.g., $E/2-\omega_c\sim 0$ in Fig. 5(c) and $E/2-\omega_c\sim -2$ in Fig. 5(d). We emphasize that this behavior, that different resonances in the single-photon spectrum have very different correlation behaviors, is unique in the whispering-gallery resonator system, and certainly does not occur in the standard JC model in the strong-coupling regime.

The presence or absence of the photon-blockade effect at the different resonances is closely related to the energy spectrum that we analyzed in Figs. 2(a) and 2(b). Since the free mode B is decoupled from the atom, its energy spectrum $E=n(\omega_c\mp|h|)$ is linear. Thus, there is no photon-blockade effect when the incident photon is resonant with the free mode. On the other hand, the spectrum of the JC mode is highly nonlinear. Thus, while a single photon on resonance with one of the JC modes is reflected, two such photons can not be simultaneously reflected since the total energy is off resonance in the two-excitation subspace.

D. Weak coupling case

In this section, we consider the photon-blockade effect in the weak coupling regime. For this purpose, we choose the same system as in Fig. 3(c), where the single-photon transmission spectrum exhibits a single dip located at the atomic resonance frequency. We consider two incident photons, both on resonance with the atom.

According to the general result (43), the second order correlation function for the two reflected photons reads

$$g_{\mathrm{R}}^{(2)}(\tau)=|1-\Gamma^2 g^2 F(\tau)|^2, \tag{44}$$

when the energy $E/2$ of each incident photon is resonant with $\Omega=\omega_c$. Using Eq. (44), we show $g_{\mathrm{R}}^{(2)}(\tau)$ for $h=0, g_a=g_b\equiv g=0.3$, and the changes of $g_{\mathrm{R}}^{(2)}(0)$ from the strong coupling case to the weak coupling case in Fig. 6. It is clear that $g_{\mathrm{R}}^{(2)}(\tau)$ displays the manifest photon-blockade effects in the weak coupling limit.

It has been shown in Ref. [27] that in a system with a waveguide side coupled to a standard Jaynes-Cummings model with a single-mode resonator, the system also exhibits a photon-blockade effect in the weak-coupling limit. However, in the system of Ref. [27], in the weak-coupling limit, the single-photon transmission peaks at the atomic resonance frequency, and photon blockade occurs for *transmitted* photons when the two incident photons are on resonance with the atom. In contrast, in the present case the photon blockade occurs for reflected photons when the two incident photons are on resonance with the atom. Thus, the presence of the free modes in the whispering-gallery mode resonator system in fact has a

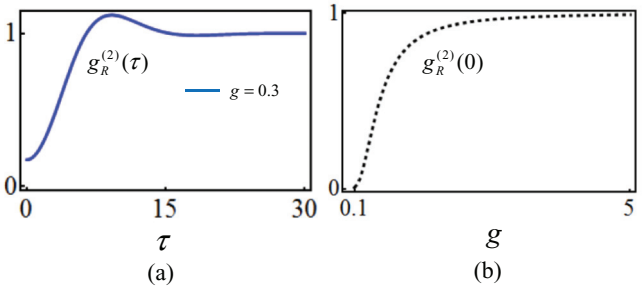

FIG. 6. (Color online) The second order correlation functions of reflected photons, where Γ is taken as units: (a) the weak coupling case $g=0.3$; and (b) the change of $g_R^{(2)}(0)$ from the strong coupling case to the weak coupling case.

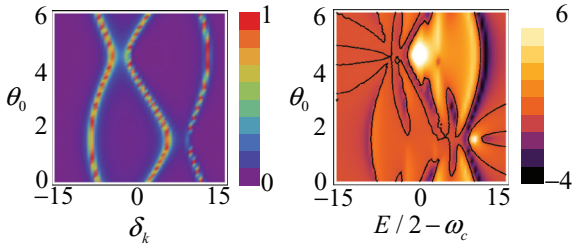

FIG. 7. (Color online) The single-photon reflection and the second order correlation functions, where Γ is taken as unity, $|h| = 5$, $\theta_h = \pi/2$, and other parameters are the same as those in Fig. 3(b): (a) the single photon reflection; and (b) the second order correlation functions $\ln g_R^{(2)}(0)$. Here, the black curves denote $g_R^{(2)}(0) = 1.0$.

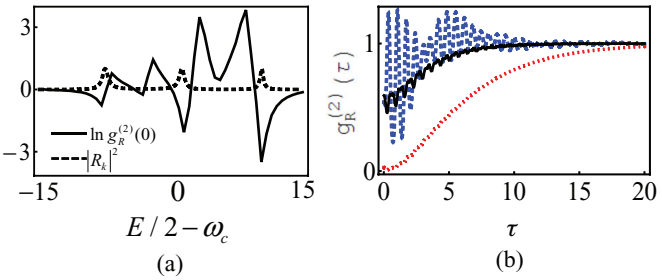

FIG. 8. (Color online) The second order correlation functions of two reflective photons, where $|h| = 5$, $\theta_h = \pi/2$, $\theta_0 = 0$, and Γ is taken as unity, (a) the solid and dashed curves denote $\ln g_R^{(2)}(0)$ and the single-photon reflection, respectively; and (b) the solid (black), dashed (blue), and dotted (red) curves denote the $g_R^{(2)}(\tau)$ for the incident resonant energies $E/2 - \omega_c = -7.39$, 1, and 10.84, respectively. Other parameters are the same as those in Fig. 3(b).

very important consequence for the transport and correlation properties of this system. The similar photon-blockade effects in the weak coupling limit have also been found recently in the bimodal system [33].

VI. RESULTS FOR THE TWO-MODE CASE

In this section, we use the general formula derived in Sec. III to study the single- and two-photon transports for the two-mode case. In the presence of the intermodal coupling, i.e., $h \neq 0$, we see in Eq. (34) that except for a very special choice of the relative phase of g_a and g_b, corresponding to one special choice of atom position, in general one can not form a photon mode that decouples from the atom. We define $\theta_0 = \arg(g_b/g_a)$. The analytic results for the single-photon intensity response function and the two-photon correlation function depend only on $\theta_0 + \theta_h$. Thus, in the numerical results, without loss of generality we fix $\theta_h = \pi/2$, and vary θ_0 from 0 to 2π.

In the two-mode case, where the atom couples to two-photon modes, both the single-photon reflection [Fig. 7(a)], and in the two-photon case, the statistics of the outgoing photon [Fig. 7(b)] become dependent upon θ_0, and hence the position of the atom. Therefore, by controlling the position of the atom, one can tune both the single-photon transport and two-photon correlation properties.

Similar to the effective one-mode case, here with the choice of parameters that place the system in the strong-coupling regime, the single-photon reflection also exhibits three peaks [Fig. 8(a), dashed line]. Unlike the effective one-mode case, however, here all three peaks exhibit the photon-blockade effect. In Fig. 8(a), we plot $g^{(2)}(0)$ for the two reflected photons, when two photons having the same energy $E/2$ are incident upon the system. We see strong resonant behavior of $g^{(2)}(0)$ at the energy corresponding to the three single-photon eigenmodes. The $g^{(2)}(\tau)$ at these three energies are plotted in Fig. 8(b), where we see a strong photon-blockade effect with $g^{(2)}(0) \ll 1$. In the two-mode case, all eigenmodes have atomic excitation and hence contribute to correlated transport.

VII. CONCLUSION

In summary, in this paper we studied the two-photon transport of the whispering-gallery-atom system by the LSZ reduction approach. We considered the cases of systems with or without intermodal mixing, and presented exact results on the second-order correlation functions of the two reflected photons, which exhibited the photon-blockade effect in both the strong coupling and the weak coupling cases. We expect the LSZ formalism may be developed to treat the photon-blockade effect in other systems as well, including the optomechanical system that was considered in [34–37].

ACKNOWLEDGMENTS

T.S. was supported by the EU under the IP project AQUTE. S.F. acknowledges the support of an AFOSR-MURI program on quantum metamaterial (Grant No. FA9550-12-1-0488).

[1] M. Rosenblit, P. Horak, S. Helsby, and R. Folman, Phys. Rev. A **70**, 053808 (2004).
[2] K. Srinivasan and O. Painter, Nature (London) **450**, 862 (2007).
[3] B. Dayan, A. S. Parkins, T. Aoki, E. P. Ostby, K. J. Vahala, and H. J. Kimble, Science **319**, 1062 (2008).
[4] T. J. Kippenberg, S. M. Spillane, and K. J. Vahala, Appl. Phys. Lett. **85**, 6113 (2004).
[5] K. Srinivasan and O. Painter, Phys. Rev. A **75**, 023814 (2007).
[6] J. T. Shen and S. Fan, Phys. Rev. A **79**, 023838 (2009).
[7] J. T. Shen and S. Fan, Phys. Rev. A **82**, 021802(R) (2010).
[8] E. E. Hach, A. W. Elshaari, and S. F. Preble, Phys. Rev. A **82**, 063839 (2010).
[9] X. Zang and C. Jiang, J. Phys. B **43**, 065505 (2010); **43**, 215501 (2010).
[10] Y. C. Liu, Y. F. Xiao, B. B. Li, X. F. Jiang, Y. Li, and Q. Gong, Phys. Rev. A **84**, 011805(R) (2011).
[11] Y. Shen and J. T. Shen, Phys. Rev. A **85**, 013801 (2012).
[12] H. J. Carmichael, *Statistical Methods in Quantim Optics I: Master Equations and Fokker-Planck Equations* (Springer-Verlag, Berlin, 2003).

[13] J. T. Shen and S. Fan, Phys. Rev. Lett. **95**, 213001 (2005).
[14] L. Zhou, J. Lu, and C. P. Sun, Phys. Rev. A **76**, 012313 (2007).
[15] L. Zhou, Z. R. Gong, Y. X. Liu, C. P. Sun, and F. Nori, Phys. Rev. Lett. **101**, 100501 (2008).
[16] H. Dong, Z. R. Gong, H. Ian, Lan Zhou, and C. P. Sun, Phys. Rev. A **79**, 063847 (2009).
[17] Y. Chang, Z. R. Gong, and C. P. Sun, Phys. Rev. A **83**, 013825 (2011).
[18] L. Zhou, Y. Chang, H. Dong, L. M. Kuang, and C. P. Sun, Phys. Rev. A **85**, 013806 (2012).
[19] J. T. Shen and S. Fan, Phys. Rev. Lett. **98**, 153003 (2007); Phys. Rev. A **76**, 062709 (2007).
[20] D. Roy, Phys. Rev. A **83**, 043823 (2011).
[21] J. Q. Liao and C. K. Law, Phys. Rev. A **82**, 053836 (2010).
[22] P. Longo, P. Schmitteckert, and K. Busch, Phys. Rev. A **83**, 063828 (2011); Phys. Rev. Lett. **104**, 023602 (2010).
[23] T. Shi and C. P. Sun, Phys. Rev. B **79**, 205111 (2009); arXiv:0907.2776 [quant-ph].
[24] T. Shi, S. Fan, and C. P. Sun, Phys. Rev. A **84**, 063803 (2011).
[25] E. Rephaeli and S. Fan, Phys. Rev. Lett. **108**, 143602 (2012).
[26] E. Rephaeli, Ş. E. Kocabaş, and S. Fan, Phys. Rev. A **84**, 063832 (2011).
[27] E. Rephaeli and S. Fan, IEEE J. Sel. Top. Quantum Electron. **18**, 1754 (2012).
[28] A. Majumdar, M. Bajcsy, and J. Vučković, Phys. Rev. A **85**, 041801(R) (2012).
[29] H. Walther, B. Varcoe, B. Englert, and T. Becker, Rep. Prog. Phys. **69**, 1325 (2006).
[30] K. M. Birnbaum, A. Boca, R. Miller, A. D. Boozer, T. E. Northup, and H. J. Kimble, Nature (London) **436**, 87 (2005).
[31] E. T. Jaynes and F. W. Cummings, Proc. IEEE **51**, 89 (1963).
[32] H. Lehmann, K. Symanzik, and W. Zimmermann, Nuovo Cimento **1**, 1425 (1955).
[33] A. Majumdar, M. Bajcsy, A. Rundquist, and J. Vučković, Phys. Rev. Lett. **108**, 183601 (2012).
[34] F. Marquardt and S. M. Girvin, Physics **2**, 40 (2009).
[35] P. Zhang, Y. D. Wang, and C. P. Sun, Phys. Rev. Lett. **95**, 097204 (2005).
[36] F. Xue, L. Zhong, Y. Li, and C. P. Sun, Phys. Rev. B **75**, 033407 (2007).
[37] P. Rabl, Phys. Rev. Lett. **107**, 063601 (2011).